INTERNATIONAL JOURNAL OF AUTOMOTIVE AND MECHANICAL ENGINEERING (IJAME)
ISSN: 2229-8649 e-ISSN: 2180-1606
VOL. 19, ISSUE 3, 9892 – 9908
DOI: https://doi.org/10.15282/ijame.19.3.2022.02.0762

ORIGINAL ARTICLE

Passive Drag Reduction of the Square Back Truck Body

A. Altaf[1], A. Omar[2,*] and W. Asrar[1]

[1]Department of Mechanical Engineering, Internatipnal Islamic Universiti Malaysia, , PO Box 10, 50728, Kuala Lumpur, Malaysia
[2]School of Aerospace andf Automotive Engineering, International University of Rabat, Parc Technopolis, Rabat-Sale, 11100 - Sala Al Jadida, Morocco.

ABSTRACT – Drag is one of the most significant factors that increase fuel consumption, followed by operating cost of the vehicle. Square-back road vehicles like trucks and buses are common and popular means of transport across the globe. In this background, it is of great research value to reduce the drag on vehicles, improve their fuel efficiency and reduce their operational cost. In this work, a simplified model of a truck was considered, and its drag was reduced by modifying its geometry using passive drag reduction devices. The passive devices used in this study were backward-facing step, fins, splitter plates/tabs, dimple, vents, and channels. These devices, of different sizes and configurations, were numerically studied using CFD software Star CCM+ at a Reynolds number of 2.4127×10^6. Drag reduction up to 9.9% was achieved, when backward-facing step was placed at the bottom rear edge of the truck. Further, multiple circular channels used on the truck's sides reduced the drag up to 6.5%, while multiple rectangular channels on the sides of the truck achieved 5.1% drag reduction. The maximum drag reduction of the fins was found to be 4.6%. In spite of these, no significant drag reduction was observed when using splitter plates/tabs, dimple and vents.

ARTICLE HISTORY
Received: 29th June 2021
Revised: 29th Aug 2022
Accepted: 18th Sept 2022
Published: 30th Sept 2022

KEYWORDS
Add on passive devices;
CFD;
Passive drag reduction;
Square back road vehicles

INTRODUCTION

The aerodynamic drag occurs in bluff bodies like trucks due to flow separation at sharp corners of the body. This phenomenon results in the formation of a large wake behind the vehicle. As a consequence, high-pressure variation occurs in that region which in turn results in high-pressure drag that dominates the total drag of the vehicle. In the case of streamlined bodies, it is possible to reduce the drag to some extent in an effective manner by changing the flow conditions (Reynolds number, Re). However, when it comes to bluff bodies with sharp corners, the drag force cannot be influenced by a change in Re. Hence, the need arises for a means to modify or manage the flow around body. Reducing large wake regions, behind such vehicles results in pressure drag reduction and less fuel consumption. Hsu and Davis [1] mentioned that $10,000 could be saved per year if a truck's drag force is reduced by 40%.

RELATED WORK

In their review article, Altaf et al. [2] highlighted the application of both active and passive drag reduction techniques upon bluff bodies. The study concluded that the passive method did not receive a lot of attention by researchers especially its application in 3D bluff bodies. In another work, Altaf et al. [3] mounted several flap configurations on the rear end of a truck as an add-on device to numerically study its effect on the total drag of the truck. They used Reynolds Averaged Navier Stokes (RANS) equations and k-Omega turbulence model. The study achieved 11.1% drag reduction with the help of elliptical-shaped flap. Vortex Generator (VG) is one of the frequently used passive flow control techniques for road vehicles. It is mostly mounted on the rear end of the vehicle to reduce drag by preventing flow separation [4-6]. Ait Moussa et al. [7] geometrically optimized bumps, on the rear end of the cabin roof in generic truck, to achieve 6-10% aerodynamic-based drag reduction out of the total drag. They used automatic combination of numerical technique and optimization where the turbulence was solved using realizable k-epsilon turbulance model.

Wang et al. [8] designed a dimpled non-smooth surface on the basis of Kriging surrogate optimization model. This surface was used for Ahmed body slant back surface. The numerical simulation using RANS and k-epsilon turbulence model achieved a maximum drag reduction of 5.2%. Sivaraj et al. [9], in their experimental study, attached base-bleed to a car model at optimized locations in order to minimize base drag. The study used two converging hollow tubes with different cross sections. The tubes sucked the air at front end and injected at the rear end. The study achieved a drag reduction of 6.2%, due to the reduction of negative pressure at the rear of the car model. Huluka and Kim [10] numerically studied using the impact of air duct system addition to Ahmed body upon pressure drag of the vehicle. They used RANS solver with Chen-Kim k-epsilon turbulence model. Different cross-sectioned ducted models were used in this study with and without chamfer. The lower surface of the duct is fixed at a constant height from lower surface of the model. The researchers observed a significant drag reduction for the ducted model in comparison to non-ducted model. In case of chamfered ducted model, the researchers achieved a drag reduction of 19.5%. Huang et al. [11] conducted the

*CORRESPONDING AUTHOR | A. Omar | ashraf_omar@uir.ac.ma

experimental and numerical investigations of the Ahmed body for aerodynamic drag with single-channel rear diffuser. The study results revealed the importance of location of the vortex and vertical diffuser angle on drag coefficient. The researchers achieved a maximum drag reduction of 5.3% for the following configuration; 10.46˚ vertical diffuser angle, 0˚ lateral diffuser angle, and 351 mm channel width. Hariram et al. [12], in their project report, discussed about several configurations to optimize drag coefficient for European tractor and semi-trailers. The configurations include adjustable truck front cab roof deflector using cargo height detection of sensor, rear flaps, splitter plate, vortex trap, leading edge fairing, air cone, trailer side panels/- skirts/-wings, wheel deflector, smooth underbody, rear flaps, extension panels, roof tapering/lowering and a combination of two or more of the above-mentioned configurations. Rossitto et al. [13] used a six component balances and Particle Image Velocimetry (PIV) measurements to assess the impact of after-body of the fastback vehicle rounding on drag force. The researchers observed the reduction of drag up to 16% for upper edge rounding, while the reduction was linked with suppression of separation over the slant surface and the length of separation region. An investigation carried out by Hachimy et al. [14] was conducted to study the accuracy of three different turbulence models (k-epsilon, k-Omega and SST) in predicting the components drag coefficient of Ahmed body model and validating the numerical results. Their results revealed that the K-omega model has acceptable results in comparison with the given experimental data.

Backward facing step is one of the widely-studied geometries for turbulence modelling, boundary layer separation and reattachment, circulatory flow, CFD benchmark studies etc. [15-23]. Though extensive literature review has been done earlier, it has not been used upon 3D bodies for drag reduction. Some research works have been published earlier on drag reduction of backward facing step by avoiding or delaying the separation process. Rajasekaran [24] reviewed and highlighted the characteristics of separation and reattachment of flow on a backward-facing step, where the separated shear layer depends upon aspect ratio, free stream turbulence intensity, boundary layer state and thickness at separation point. The study concluded that it is possible to avoid or reduce the flow separation of backward facing step through geometric modification. Rectangular tabs, located at the edge of backward facing step, were used by Park et al. [25] to reduce the drag by limiting reattachment length. Kumar et al. [26] studied the flow over skewed steps for aerodynamic applications of road vehicles. The researchers examined both drag and pressure distribution on surface for forward facing step, backward facing step and a combination of both forward and backward facing steps under various step inclinations. The authors concluded that the coefficient of drag got mainly influenced by step geometries i.e., when step inclination decreases, the coefficient of drag decreases as well.

Though there have been several research works conducted upon the application of passive techniques to reduce aerodynamic drag of squared back road vehicles, there is no study conducted yet, to the best of researcher's knowledge about the application of backwards step in drag reduction process. This research gap inspired the current study authors to propose 'backward facing step' as one of the proposed add on devices to minimize the total drag of square back road vehicles such as trucks and buses. Backward facing step has multiple salient features such as simplicity of design, ease of manufacturing and the ability to reattach separated flow. Due to these reasons, it is considered as one of the simple and effective passive drag reduction techniques to be adapted in future trucks and buses' design trends. The work is extended to study other add-on devices especially fins, splitter plates/tabs, dimple, vents, and channels. A road vehicle's drag reduction is linked with its design optimization. The future trends should look for more enhancements in vehicle design and innovate new concepts to reduce the vehicle drag [27].

RANS EQUATIONS AND K-OMEGA TURBULACE MODEL

The steady Reynolds Averaged Navier Stokes equations (RANS) [28] for the modeling of turbulent flows are given by

$$\bar{u}_j \frac{\partial \bar{u}_i}{\partial x_j} = -\frac{\partial \bar{p}}{\partial x_i} + v\frac{\partial^2 u_i}{\partial x_j \partial x_j} - \frac{\partial \tau_{ij}}{\partial x_j}$$
$$\frac{\partial \bar{u}_i}{\partial x_j} = 0 \tag{1}$$

where τ_{ij} is the Reynolds stress and expressed as $\tau_{ij} = \overline{u'_i u'_j}$. The k-omega turbulence model relations are expressed by Wilcox [29] as

$$\frac{\partial}{\partial t}(\rho k) + \frac{\partial}{\partial x_j}(\rho u_j k) = \rho \tau_{ij}\frac{\partial u_i}{\partial x_j} - \beta^* \rho k\omega + \frac{\partial}{\partial x_j}\left[\left(\mu + \sigma^* \frac{\rho k}{\omega}\right)\frac{\partial k}{\partial x_j}\right]$$
$$\frac{\partial}{\partial t}(\rho \omega) + \frac{\partial}{\partial x_j}(\rho u_j \omega) = \alpha \frac{\omega}{k}\rho \tau_{ij}\frac{\partial u_i}{\partial x_j} - \beta \rho \omega^2 + \sigma_d \frac{\rho}{\omega}\frac{\partial k}{\partial x_j}\frac{\partial \omega}{\partial x_j} + \frac{\partial}{\partial x_j}\left[\left(\mu + \sigma \frac{\rho k}{\omega}\right)\frac{\partial \omega}{\partial x_j}\right] \tag{2}$$

The complete descriptions of the K-omega turbulance model relations and their coefficents can be found in Wilcox [29].

METHODOLOGY

The current study is an extension of previous work on the model named 'MAN TGX series' [3]. Figure 1 shows the dimensions of the scaled model. It is a common practice to simplify the geometry since it is complex to add individual contributions to every component of the truck [3]. The key simplifications made to the scaled model are given herewith.

i. Simplified geometry: the shapes of cab, appendages, underbody etc. are not considered, since the major part of the drag, in case of bluff bodies, is contributed by the frontal area.

ii. Both cab and trailer are considered to be one continuous segment.

iii. The circular geometry of tyres is simplified to rectangular shape near road in order to reduce the computational expense and rule out the effect of rolling motion of the truck.

In previous work of the current study, validation study was carried out and a flap, mounted at the rear of the truck, was used as an add-on device to reduce the drag. In current work, the truck shape is modified by including the rear edge backward facing step (Figures 2, 3 and 4) or fins (Figure 5) or splitter plates/tabs (Figure 6) or dimples (Figure 7) or vents and channels (Figures 8 and 9).

Then the computed drag coefficient of the modified trucks is compared with the drag of baseline model [3]. A common highway speed of 30 m/s (108 km/h, $Re = 2.4127 \times 10^6$) is used for all the cases presented in this study. The scaled model of 16% was used throughout the numerical work. The used physics and meshing parameters are summarized in Table 1.

Table 1. Physical and meshing Parameters

Physcial / Meshing properties	Parameters
Flow characteristics	Steady, Stationary, incompressible, turbulent, segregated flow model, 3D RANS
Solver type	Pressure-based
Turbulance model	k-omega
Inlet flow velocity	30 m/s
Outlet pressure	1 atm
Volume Mesh	Polyhedral
Boundary layers	Prism
Prism layers stretching	1.2%
Prism layers thickness	0.0236 m
Number of prism layers	10

Modified Models with Backward Facing Step

A generic backward facing step is shown in the Figures 2 to 4 which has height (h) and width (w) parameters as indicated in Figure 2. Both the parameters are expressed in terms of turbulent boundary layer thickness (δ). This form of backward facing step is added at different locations of rear of the baseline truck. Further, a backward facing step is added at both top and bottom of the truck separately and together, to isolate the effects of placing it at these locations individually. The researchers investigated different configurations of backward facing step sizes too by varying 'h' and 'w' in the range of 1.5δ, 2δ and 2.5δ in different combinations. A total of 18 backward facing step geometries was examined in this study.

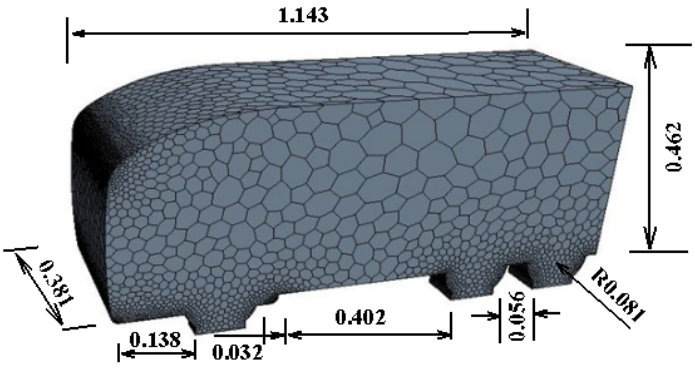

Figure 1. Dimensions (in meter) and surface mesh of scaled model

Modified Models with Fins

Fins, the thin-curved attachments, are ordinarily used in producing thrust or providing steering control and stabilization. Fishes possess heavily streamlined bodies and make use of fins to propel themselves through water. In this

background, it has been hypothesized that using a fin may increase the energy of flow and accelerate it. Fin is designed using two straight lines at an angle for leading edge, and a spline for trailing edge, as shown in Figure 5(a). Fins can be placed either individually or in a series on the roof of the truck as shown in Figure 5(b). A total of six different configurations of fins was simulated in this study based on varied height, length and spine definitions. All the tested configurations are shown in Table 2.

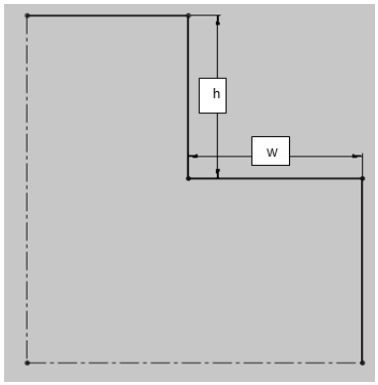

Figure 2. Backward Facing Step (BFS).

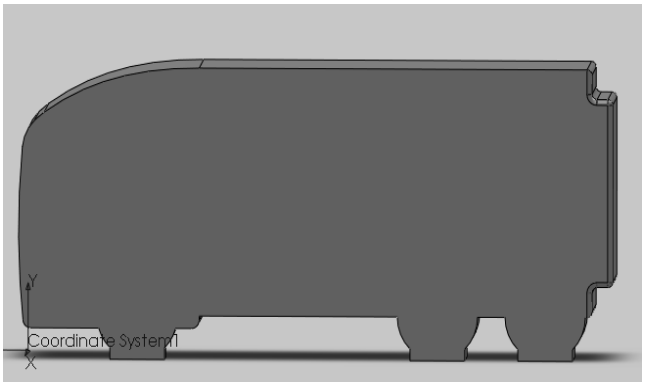

Figure 3. Truck with top and bottom (BFS).

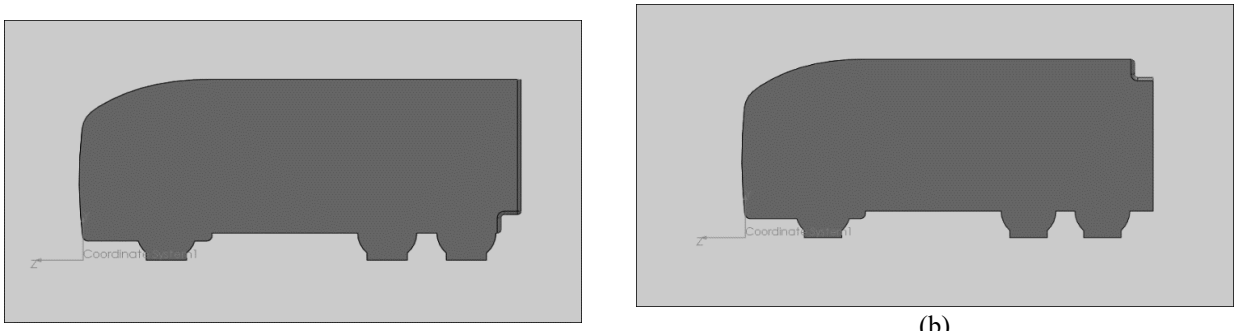

(a) (b)

Figure 4. Backward Facing Step (BFS) at (a) top and (b) bottom only.

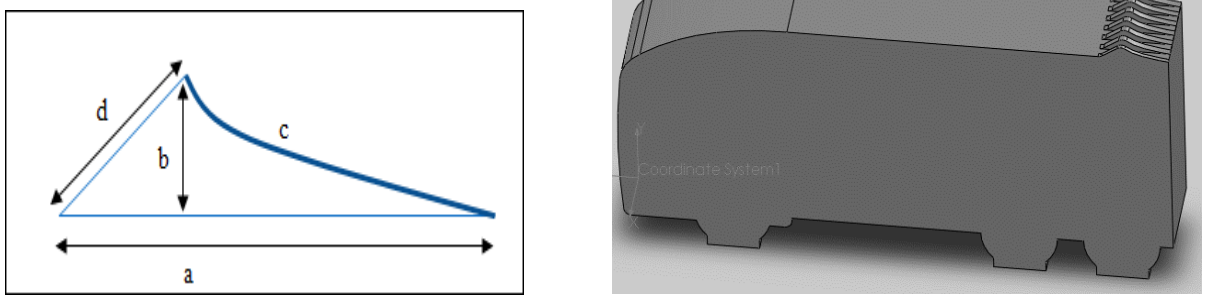

(a) Design of Fin (b) Series of fins on the roof of truck

Figure 5. Modified models with fins.

Table 2. Different configurations of fins.

Name	Configurations (m)
Fin 1	a = 0.150, b = 0.030, c = 0.10, d = 0.04, n=7
Fin 2	a = 0.193, b = 0.003, c = 0.10, d = 0.06, n=7
Fin 3	a = 0.175, b = 0.069, c = 0.12, d = 0.04, n=7
Fin 4	a = 0.173, b = 0.017, c = 0.09, d = 0.05, n=7
Fin 5	a = 0.150, b = 0.027, c = 0.10, d = 0.04, n=7
Fin 6	a = 0.150, b = 0.030, c = 0.10, d = 0.04, n= 7

Modified Models with Splitter Plates/Tabs

Gilieron and Kourta [30] studied about drag reduction caused by splitter plates on Ahmed body; whereas Park et al. [31] found that the maximum height of splitter plates should be that of the thickness of boundary layer. Therefore, in current work, the height of the splitter plates is maintained constant at 0.02m. The splitter plates of the rectangular cross-section are placed along the side of the truck. In one case, only one row of 23 equidistant splitter plates is used whereas in the second case, two identical rows are used at a distance. The plates used in this study had a length of 0.08m and width of 0.02m.

Further, triangular tabs are placed at the rear end of roof. Again, the height was maintained at 0.02m and the altitude of cross-sectional triangle was 0.01m. Some of the examples of these configurations are shown in Figure 6. In this study, three configurations of splitter plates/tabs were examined.

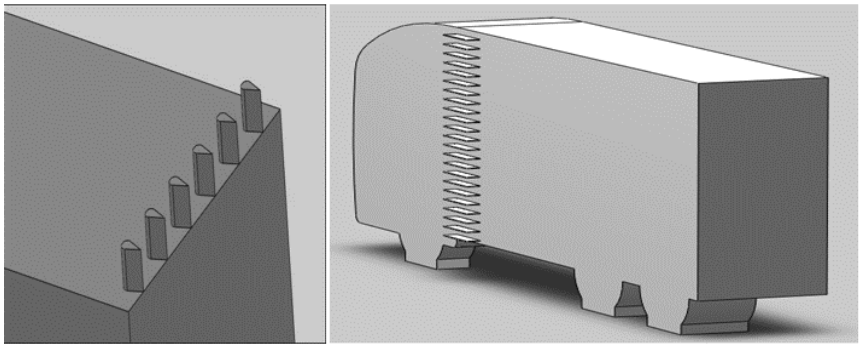

Figure 6. Configurations of splitter plates/tabs.

Modified Models with Dimples

Dimples or indentations, similar to the ones present in golf balls, are used for early transition of the flow from laminar to turbulent. This phenomenon delays or prevents the separation of flow. Further, this also reduces the drag considerably. Small spherical dimples, of radius 0.02m and depth 0.01 m, are regularly placed in the cab as shown in Figure 7.

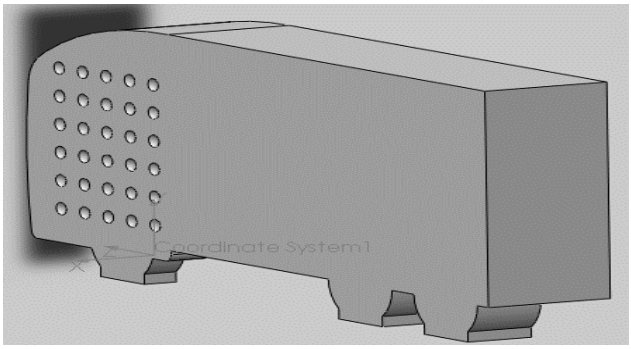

Figure 7. Dimples on truck.

Modified Models with Vents and Channels

Vents are nothing but holes straight through the body of the truck, whereas a channel is an external vent that partially intersects the truck and creates a corrugated structure. The cross-section of the vent or channel can strongly influence the intake of the flow and consequently its efficiency too. Circular, triangular, and rectangular cross-sectional vents were designed in this study with radius values being 0.015m, side 0.02m and side 0.02m, respectively as shown in Figure 8.

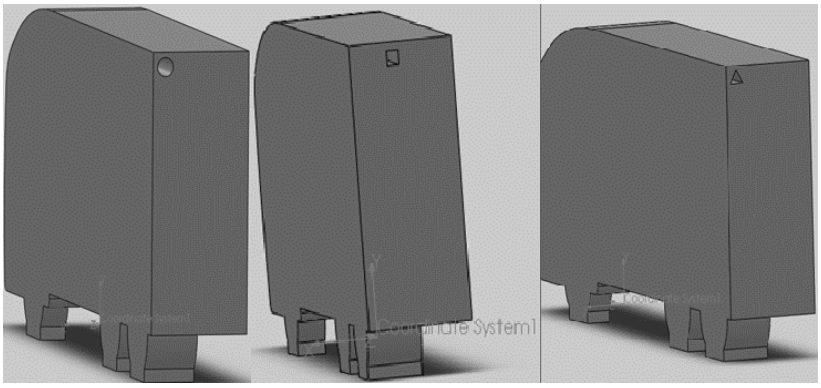

Figure 8. Sample shapes of vents.

Suryanarayana et al. [32] too studied about the vent through the center of the truck body. The cross-sectional area of the vent varies from 0.75% to 2.25% of the frontal area of the truck, and the dimensions are given in Table 3.

Table 3. Dimensions of the vents right through the middle of the truck

Model	Dimensions (m)
full truck with 2.25% vent	r = 0.037
full truck with 1.5%	r = 0.030
full truck with 0.75%	r = 0.021

External channels of different shapes, depths and widths i.e., along the side of the truck and its roof were also designed and simulated. The study used different channel sizes too, that run across the length of the truck on roof and along the sides as shown in Figure 9 and Table 4. The spacing between the channels is maintained equal. A total of nine vent cases and seven channel configurations was simulated in this study.

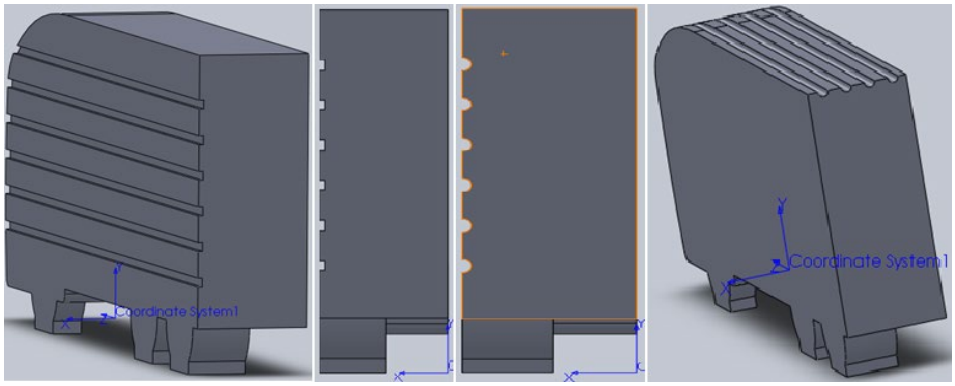

Figure 9. Samples configurations of channels.

Table 4. Dimensions of channels used.

Model	Dimensions (m)
External Rect. channel 1	Width = 0.070 and depth 0.02
External Rect. channel 2	Width = 0.015 and depth 0.013
External Circular channel on roof	Radius = 0.013, depth = 0.02
External Circular channel on sides	Radius = 0.013, depth = 0.02

Simulation Setup and Meshing

The current study used SolidWorks 2010 from Dassault Systemes to develop the CAD models. Then, the developed models were imported to CFD commercial software Star CCM+ for numerical analysis. Computational domain was generated by creating an enclosure with dimensions as follows; 10L from inlet to the nose of the model, 20L from rear end of the model to outlet and 8L for both sides and the roof of the truck to enclosure walls and roof, respectively. Here, L denotes the overall length of the truck. The road was assumed to have smooth surface. Star CCM+ is preloaded with different surface and volume mesh models based on individual problems that can be used either as standalone entity or in combination with others. In current study, surface remesher, polyhedral mesher and prism layer mesher were used [33]. Close to the surface, the prism layers were used to model the boundary layer, where the growth rate and the total number of layers were set to 1.2 and 10, respectively. The thickness of the prism layer is determined to be 0.0204m whereas the minimum thickness is of 0.002m. Polyhedral mesh, with a growth rate of 1.5%, was used for the volume outside boundary layer. The meshing parameters are presnted in Table 1. The mesh was refined at both front and back sides of the truck to capture the details of high gradient flow regions so as to enhance the drag predication as shown in Figure 10. As shown

in Table 3, the current study used steady three-dimensional Reynolds Averaged Navier Stokes (RANS) equations with K-Omega turbulence model.

The authors conducted grid independency test to determine the validity of the results. Grid independency is a significant issue in CFD simulations since it can affect the accuracy of the results. In general, grid independency tests are performed by running the same simulation tests using meshes of different densities. This helps in determining the significance between the results and grid characteristics.

Grid independency test was conducted with varied number of cells on the basis of coarseness and fineness of the grid. The tests were performed on baseline model, and the criteria selected was 'drag coefficient'. The results of the tests are given in Table 5. It can be observed that 12% was the maximum change occurred when the mesh was changed from fine to coarse and the number of cells was almost doubled. Medium mesh drag coeffient agreed well with the result obtained by Altaf et al. [3], therfore the medium mesh was used throughout the study.

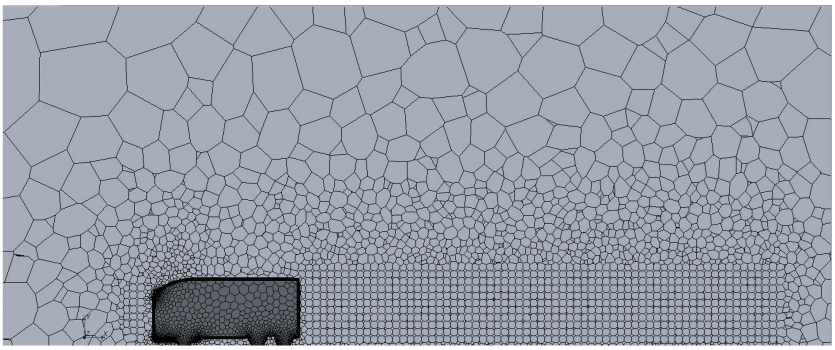

Figure 10. Finer meshes in front and at the back of the truck.

Table 5. Grid independent test.

Mesh	No. of cells	Drag coefficient
Coarse	298857	0.734
Medium	331901	0.640
Fine 1	471249	0.637
Fine 2	583726	0.660

RESULTS AND DISCUSSION

Baseline

The simulation results for the baseline model are shown in Figures 11 to 14. Figure 11 shows the side view of the truck against the symmetry plane. The figure portrays the velocity magnitude plot of airflow past the truck. The four vertical lines are positioned at x = 0.042, 0.21, 0.37 and 0.86 m from the rear of the truck. It can be understood from the figures that a wake is created at second line (x = 0.21 m) with a centre. It is useful to visualize both pressure and velocity in the cross-section of wake so as to find the possible techniques that can minimize these entities. Figure 12 shows velocity distribution for a cut plane with resolution (100 × 100 points) at 0.21 m from the rear of the truck. Both pressure distribution and velocity flow on the cut-plane are shown in Figure 13. Based on the baseline pressure distribution on cut-plane, it is clearly evident that there exist two concentrated low-pressure regions, with each one reaching nearly -115 Pa. This is supported by the velocity flow vectors that exhibit two counter-rotating vortical regions. Further, this flow occurs towards the back of the truck ('scooping in') as shown in the figures which display the airflow pattern past the rear of the truck. It can be concluded from pressure distribution and velocity flow results around the truck that wake vortices are largely responsible for truck's drag. Figure 14 shows the top view of the pressure contours at a height of 0.25 m from the road – or on a plane, almost half the height of the truck. Two circular negative pressure regions can be clearly seen at the rear of the truck.

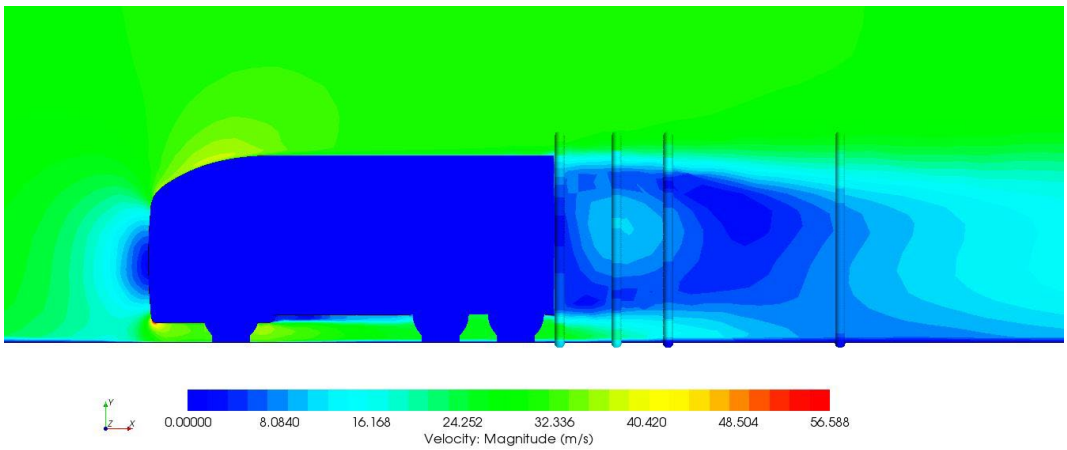

Figure 11. Wake behind the baseline Model with 'x' locations.

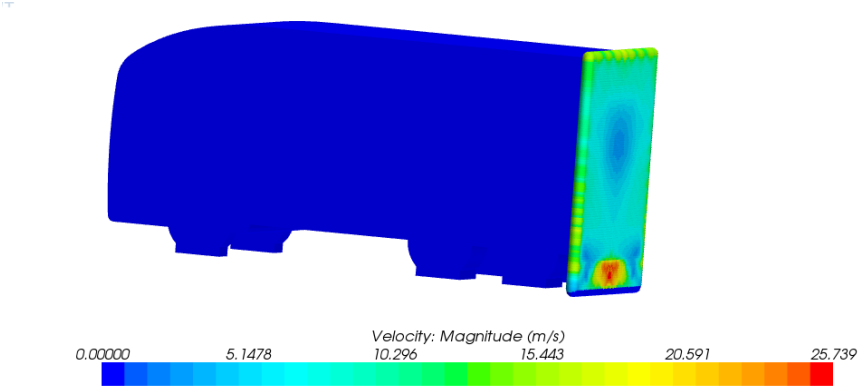

Figure 12. Velocity distribution for the location of a cut plane at a distance of 0.21m from the rear of the truck.

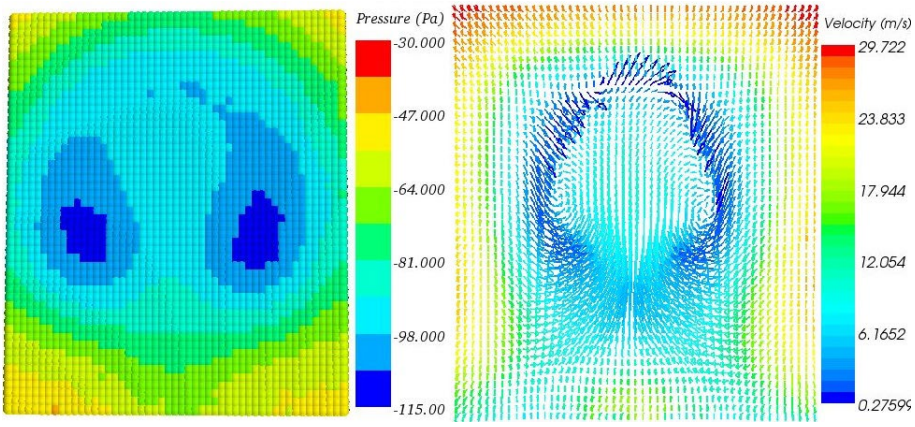

(a) (b)

Figure 13. (a) Pressure distribution and (b) velocity flow on the presentation grid at a distance of 0.21 m from the rear of the truck.

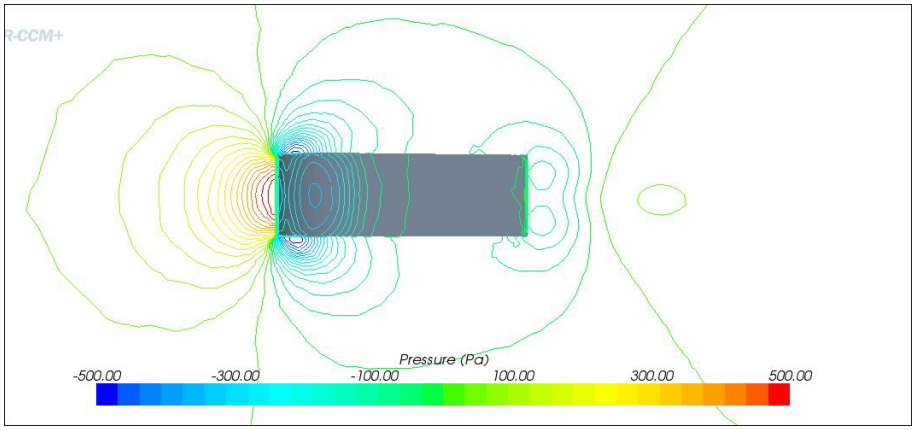

Figure 14. Pressure contours around the truck-top view at a height of 0.25 m from the road.

Geometry Modification: Backward Facing Steps

Figure 15 shows the wake behind the truck with a backward facing step sized at h= 1.5δ and w= 1.5δ at top and bottom surface of the rear end of the truck. There is a considerable reduction observed in the size of wake due to fragmentation of the large wake into smaller regions with circulating flow. Further, drag reduction was also observed in this case up to 8.87%. It should be noted that this phenomenon is a result of individual top and bottom backward facing steps that sum up together to reduce the drag. However, top and bottom backward facing steps may have different effects when considered separately.

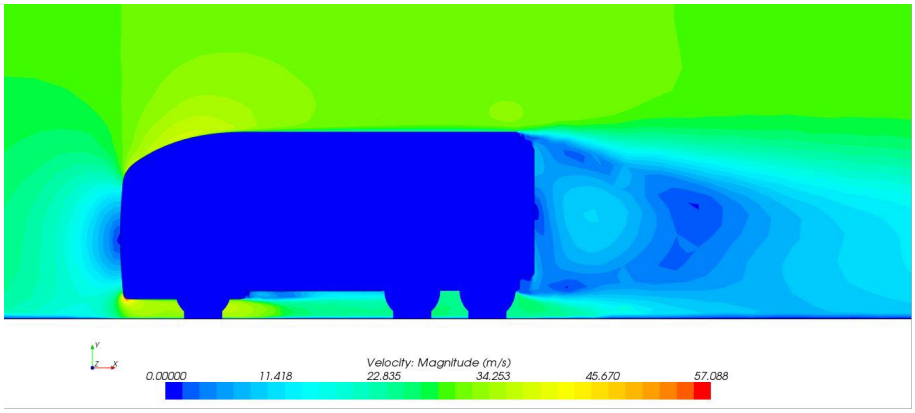

Figure 15. Wake behind truck - both top & bottom backward facing steps (1.5δ,1.5δ config.)

Figure 16(a) shows the velocity vectors inside the backward facing step sized at h= 2δ and w= 1.5δ when using top backward facing step alone. Figure 16(b) shows the velocity vectors at top backward facing step, when both top and bottom backward facing steps are used together with same dimensions. It can be inferred that when top backward facing step is used alone, two co-rotating circular flow regions exist. On the other hand, when both top and bottom backward steps are used together, one distinct circulatory flow region can be observed. However, in both the cases, the circular flow at the top step rotates in the opposite direction of main wake flow. This scenario results in both cancellation and fragmentation of the main wake, behind the truck, thereby reducing the overall drag. There was a reduction in drag up to 6.35% in top-alone configuration. When used at both top and bottom, the drag got reduced up to 8.7%. This infers that in spite of the distant relationship between top and bottom backward facing steps, their effects on each other cannot be ignored due to significant change in overall drag reduction. When backward facing step of the same dimension was used, only at the bottom of the truck, the drag got reduced up to 8.1%.

Since top and bottom backward facing steps depend upon the flow, different simulation scenarios were tested such as top only, bottom only and top and bottom backward facing step configurations using different sizes. The overall drag reduction results are shown in Table 6. The table also indicates the combination and sizes of the backward facing step that yielded the maximum drag reduction. The velocity magnitude plot of airflow and the pressure distribution, at the back of the truck, for the above-mentioned cases are shown in Figures 17 to 19.

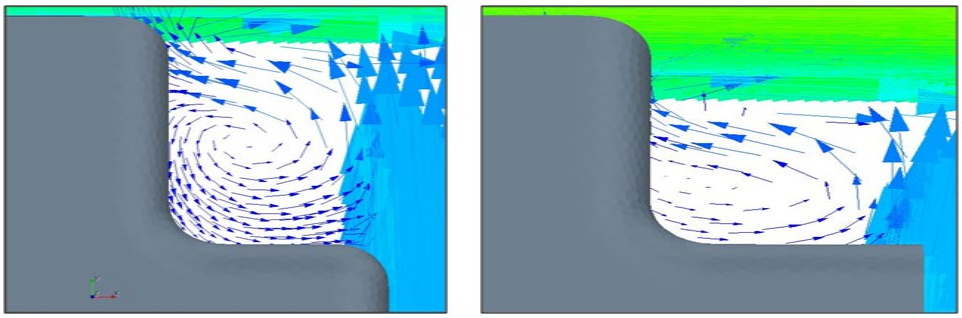

(a) Both top &bottom backward facing step (b) Top only backward facing step

Figure 16. Backward facing step (2δ,1.5δ config.).

Table 6. Percentage Drag reduction for different configurations and locations.

Step Sizes (h, w)	Percentage of drag reduction		
	Top only	Bottom only	Top and bottom
(1.5 δ, 1,5 δ)	7.13	8.24	8.88 (max)
(2 δ, 1.5 δ)	6.35	8.10	8.71
(2.5 δ, 1.5 δ)	6.45	5.22	7.66
(2 δ, 2 δ)	9.01 (max)	9.92 (max)	8.10
(1.5 δ, 2 δ)	7.34	8.75	7.86
(2.5 δ, 2 δ)	7.14	8.46	7.92

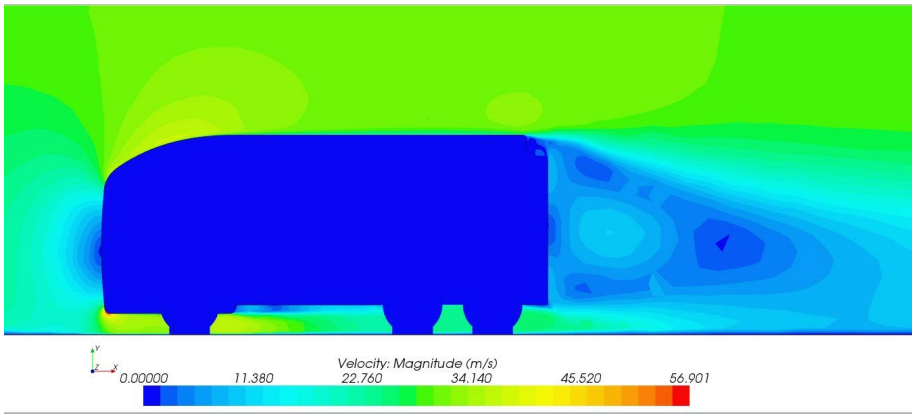

Figure 17. Velocity profile for case with max drag reduction with top only backward facing step (2δ, 2 δ config.)

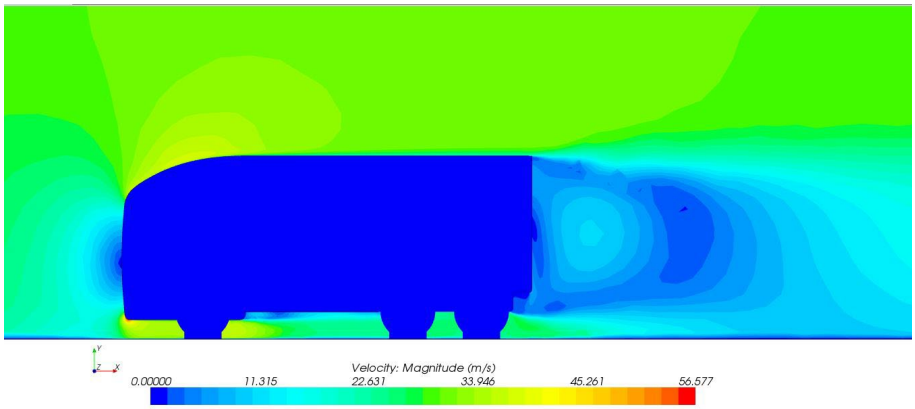

Figure18. Velocity profile for case with max drag reduction with bottom only backward facing step (2δ, 2 δ config.).

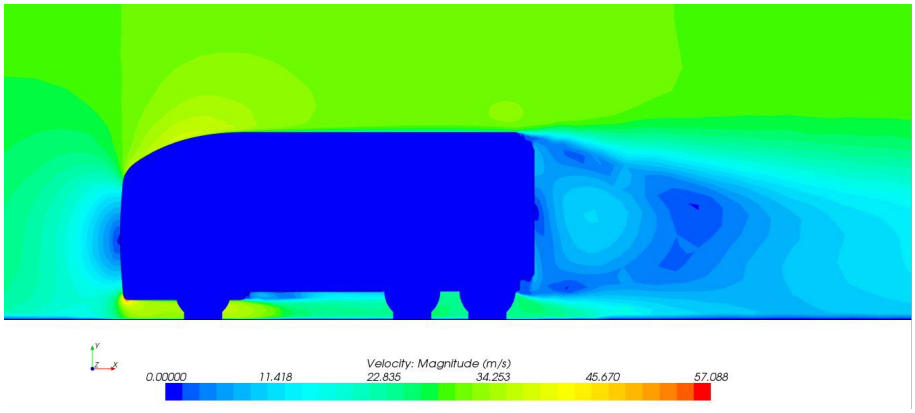

Figure 19. Velocity profile for case with max drag reduction with both top and bottom backward facing steps (1.5δ, 1.5 δ config.).

In Table 6, it is interesting to find that the maximum drag reduction was obtained from top only and bottom only configurations when using the backward facing step sized at h = 2δ and w= 2δ. Further, the maximum drag reduction was obtained when using both top and bottom steps with a backward facing step size of h =1.5δ w= 1.5δ instead. The total maximum drag reduction obtained was 9.92% in case of bottom-only backward facing step. This might be attributed to counter rotating flow, past the bottom backward facing step which has higher velocity than the counter rotating flow produced by top backward facing step. This way, more interference is found with the main wake. Further, higher velocity observed in this scenario might be due to higher speed flow, past the underbody of the truck than the roof. In addition, it can be inferred that the increasing of the backward facing step size is not improving the drag reduction. To support this, no high drag reduction was found at a size of h =2.5 δ and w= 2 δ i.e., maximum area and perimeter, for the simulated backward facing step. This could be due to increase in surface area as a result of trade-off between drag reduction by fragmenting the wake and increased drag due to skin friction.

Geometry Modification: Fins

As the fins are placed on the roof of the truck, it is important to investigate their impact on flow, past the rear of the truck. The velocity of the flow is given in Figure 20. Fins tend to accelerate the flow slightly at the top corner of the truck than the baseline case. This is indicated by green arrows that extend past the corner and go downwards. Figure 21 shows the results of rear cut-plane at distance of 0.21m from the rear of the truck , which describe the impact of fins upon wake dynamics. It can be understood from Figure 21 that the velocity vectors behind truck seem to be highly symmetrical than the baseline. Also, low-pressure blue region seems to have dissipated, possibly due to slightly accelerated flow, past the top corner.

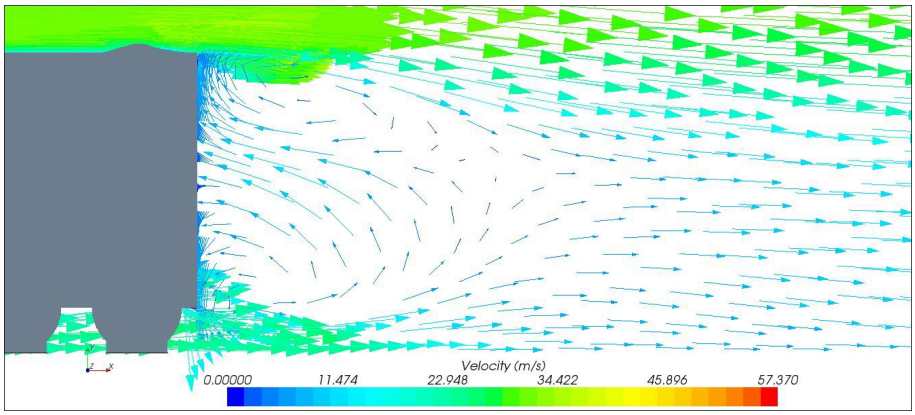

Figure 20. Velocity vectors around truck with fin.

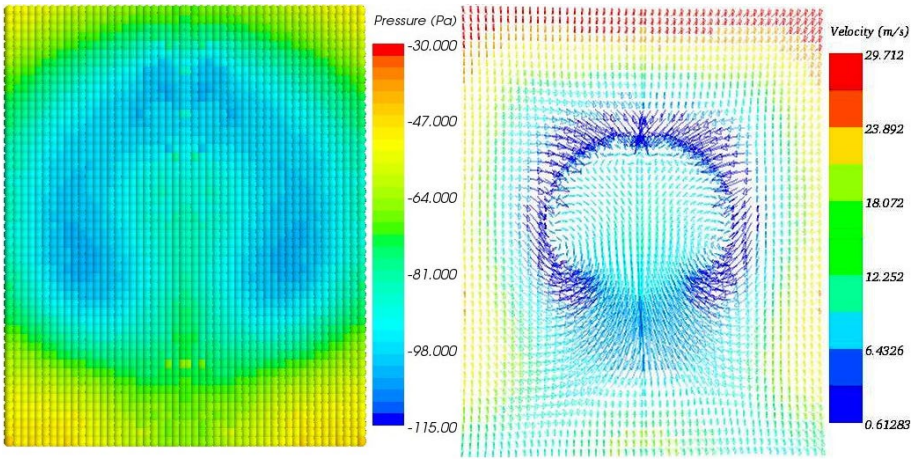

Figure 21. Pressure distribution and velocity flow at the back on presentation grid at a distance of 0.21m from the rear of the truck.

Geometry Modification:Splitter Plates/Tabs

Figures 22 and 23 show the visualizations of pressure and velocity flow field at a height of 0.25 m from the road. Dual-column splitter plates, present on the side of the truck, yielded the highest drag reduction. Further, they are also oriented to affect the flow along the side of the truck.

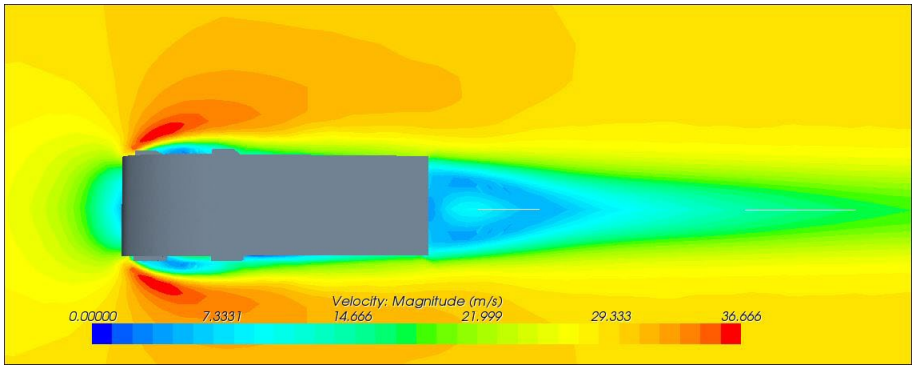

Figure 22. Velocity plot around truck - top view at a height of 0.25m from the road.

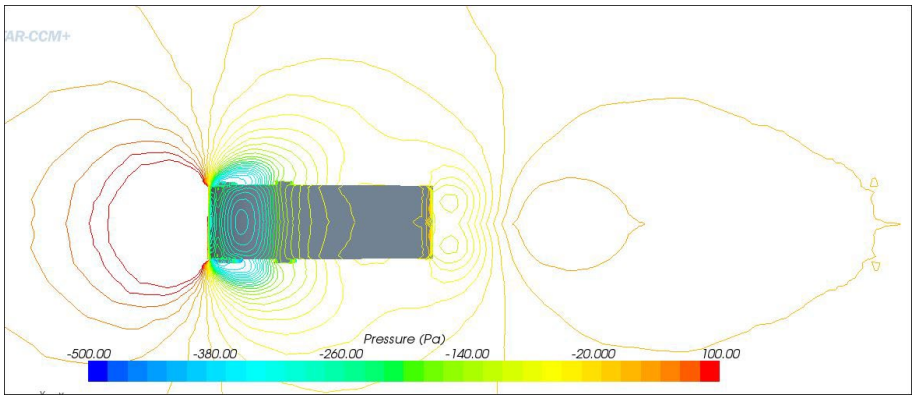

Figure 23. Pressure contours - top view at a height of 0.25m from the road.

In comparison with velocity flow around the baseline truck, it can be observed that low velocity bubbles got created near the first row of splitter plates. This is attributed to the interference in normal flow, caused by the plates. The second row recorded no such effect on the flow. However, in pressure distribution figure, the second row of plates record a bubble of slightly higher pressure.

Geometry Modification: Dimples

The dimples altered the flow along the sides of the truck alike splitter plates. Thus, it is imperative to look at the flow, past the sides of the truck than at the rear of the truck. Figures 24 and 25 show the velocity magnitude and pressure contours at a height of 0.25 m from the road.

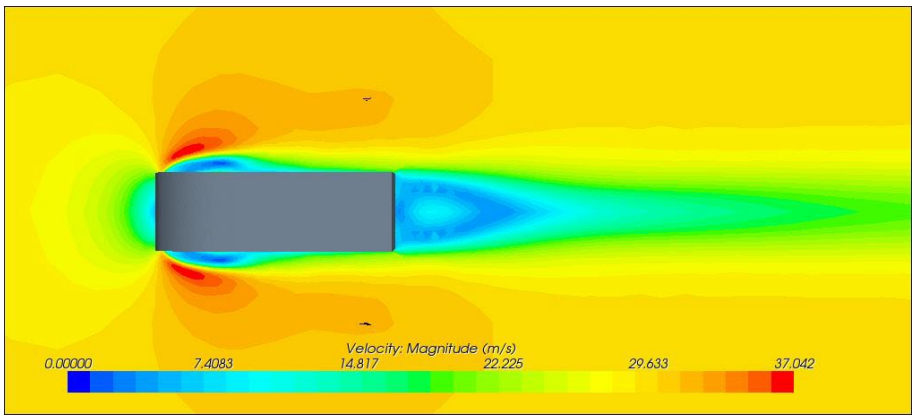

Figure 24. Velocity plot - top view at a height of 0.25m from the road.

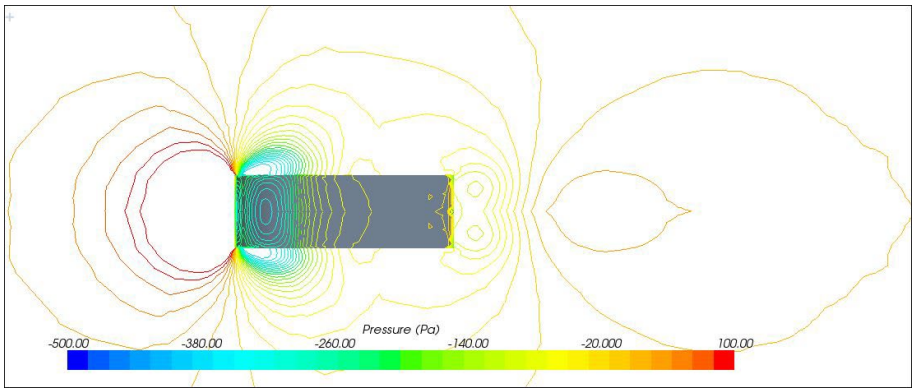

Figure 25. Pressure contours - top view at a height of 0.25 m from the road

It can be observed from the figures that dimples exercise a minimal effect upon the overall flow, past the truck. Dimples exhibit a primary characteristic i.e., to reduce the velocity of the flow near leading corners of the truck. This infers the creation of a slightly smaller and diluted wake at the back of the truck. Further, the phenomenon can be seen clearly, when comparing pressure distribution graphs in Figures 14 and 25. Two circular regions exhibited a small size and high pressure. To support this stance, Figure 26 shows the pressure distribution and velocity flow for cut-plane at a distance of 0.21m from the rear of the truck. It can be inferred from the figures for cut-plane pressure and velocity flow that wake size is much smaller and there is no pressure drop to low levels, as seen in the baseline model, indicated by dark blue regions.

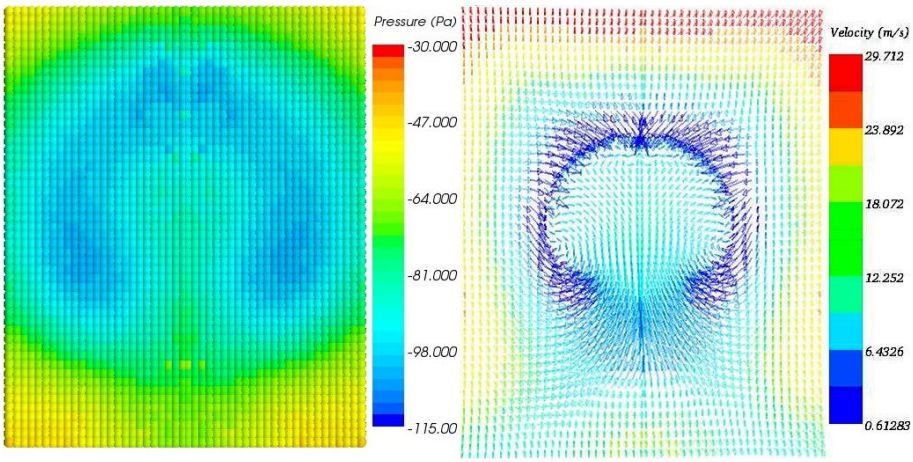

Figure 26. Pressure distribution and velocity vectors on presentation grid at a distance of 0.21 m from the rear of the truck.

Geometry Modification: Vents and Channels

Once again, both vents and the channels mostly change the flow along the side of the truck. Figures 27 and 28 show the pressure distribution and velocity flow, around the truck at a height of 0.25 m from the road, for the best case of vents. In case of velocity flow around the truck, it can be observed that the truck seems to have been enveloped in a low velocity flow, all along the sides and finally ended in wake. This is basically a large scale effect observed in splitter plates since splitter plates, extended along the length of the truck, essentially turns it into a channel. At the beginnings of the sides, low velocity regions exist alike the results of the splitter plates. Figure 29 shows the results for pressure distribution and

velocity flow on cut-plane behind the truck. The velocity vector plot indicates that the width of wake got reduced resulting in narrow-shaped ellipse. The pressure distribution was found to be even with higher pressure values than the baseline model.

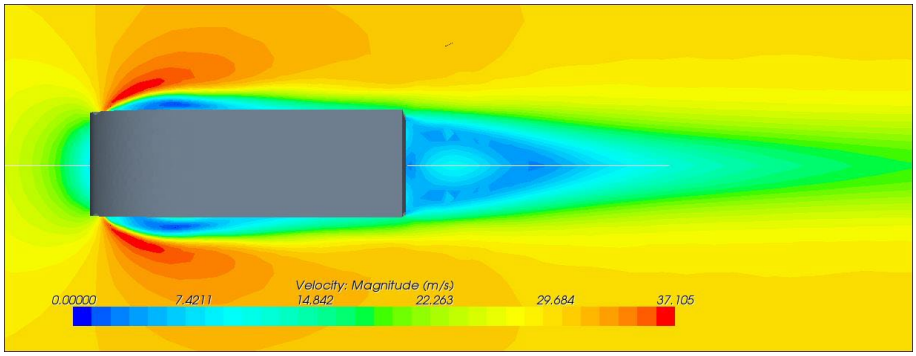

Figure 27. Velcity flow around truck - top view at a height of 0.25 m from the road.

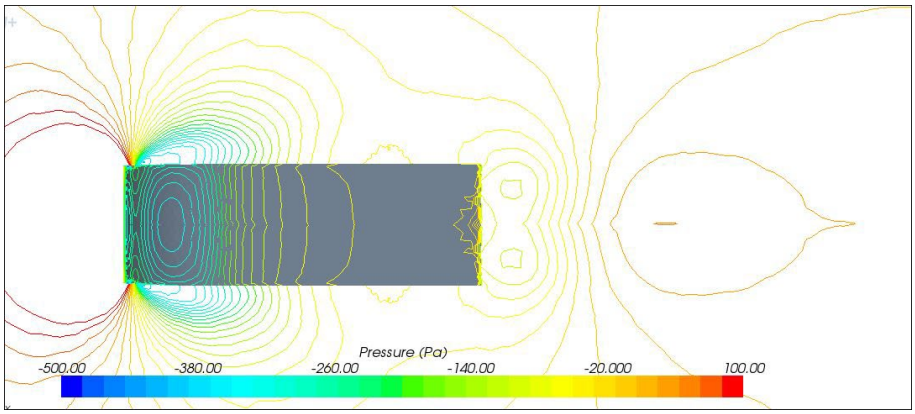

Figure 28. Pressure contours around truck with channels - top view at a height of 0.25m from the road.

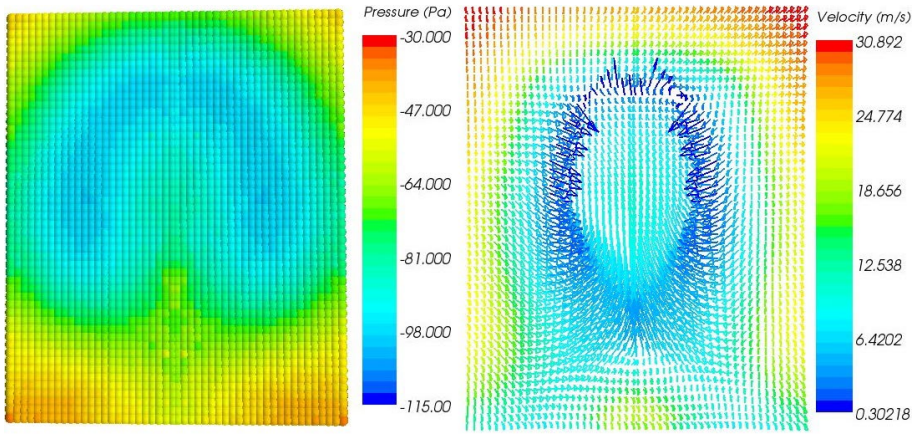

Figure 29. Pressure distribution and velocity vectors in presentation grid at a distance of 0.21 m from the rear of the truck.

SUMMARY OF THE RESULTS

Table 7 summarizes all the configurations of add-on devices that were simulated in this study and the percentages of drag reduction achieved in each case. It is interesting to note that 17 out of 18 cases of backward facing steps yielded the highest drag reduction than the tested add-on devices. The highest drag reduction of 9.92% was recorded for backward facing step, case 4. Amongst the rest of the tested add-ons, multiple circular channels on side of the truck achieved the highest drag reduction of 6.506% followed by multiple rectangular channels on sides of the truck with the highest drag reduction of 5.108%. These channels vertically exist in shipping container trucks than in a horizontal fashion. Significant drag reduction can be achieved if the channels are rotated horizontally. The maximum drag reduction achieved when using fins, vents, dimple, and splitter plates were 4.644%, 2.632%, 2.32% and 1.703%, respectively.

Table 7. Summary of results.

Model	Configuration	C_D	% decrease in C_D
Baseline		0.646	
Backward facing steps 1 (h= 1.5δ, w= 1.5δ)	Top Only		7.13
	Bottom Only		8.24
	Top and Bottom		8.88 (max)
Backward facing step 2 (h= 2δ, w= 1.5δ)	Top Only		6.35
	Bottom Only		8.10
	Top and Bottom		8.71
Backward step 3 (h= 2.5δ, w= 1.5δ)	Top Only		6.45
	Bottom Only		5.22
	Top and Bottom		7.66
Backward facing step 4 (h= 2δ, w= 2δ)	Top Only		9.01 (max)
	Bottom Only		9.92 (max)
	Top and Bottom		8.10
Backward facing step 5 (h= 1.5δ, w= 2δ)	Top Only		7.34
	Bottom Only		8.75
	Top and Bottom		7.86
Backward facing step 6 (h= 2.5δ, w= 2δ)	Top Only		7.14
	Bottom Only		8.46
	Top and Bottom		7.92
Fins	Fin1	0.618	4.334
	Fin2	0.621	3.870
	Fin3	0.629	2.632
	Fin4	0.616	4.644 (max)
	Fin5	0.621	3.870
	Fin6	0.624	3.406
Splitter plates	Triangular splitter plates roof	0.641	0.774
	Single row splitter plates	0.635	1.703 (max)
	Double row splitter plates	0.635	1.703 (max)
Dimples	Radius 0.02m and depth of 0.01m	0.631	2.322
Vents	full truck with 2.25% vent	0.638	1.238
	full truck with 1.5%	0.636	1.548
	full truck with 0.75%	0.638	1.238
	Single rect. vent	0.630	2.477 (max)
	Single tri. vent	0.649	-0.450
	Single circular vent	0.629	2.632
	Single circular vent top edge	0.631	2.322
	Single circular vent bottom edge	0.632	2.217
	3 circular vents	0.631	2.322
Channels	Multiple circular on sides	0.604	6.506 (max)
	Multiple circular on roof	0.623	3.560
	Single rect. on sides	0.634	1.858
	Double rect. on sides	0.620	4.025
	Single rect. on roof	0.638	1.238
	Multiple rect. on sides	0.613	5.108
	Multiple rect. (smaller)	0.623	3.560

CONCLUSION

In this study, a simplified TGX MAN truck model was simulated at 30 m/s to establish a baseline drag, experienced by bluff bodies on long haul journeys. Backward facing step, fins, splitter plates/tabs, dimple, vents, and channels were used as passive drag reduction devices so as to reduce the total drag on the truck, by fragmenting the wake behind it. Different sizes and configurations of the devices were studied, and the results indicate the dependence of flow past passive drag devices of the truck. A maximum drag reduction of 9.92% was obtained at the backward facing step sized at h = 2 δ and w= 2δ at the bottom of the truck. The results also infer the existence of a trade-off between drag reduction by wake minimization and drag increase due to skin friction for large-size backward facing step. When using fins, the maximum drag reduction achieved was 4.8%. Multiple circular channels, on the side of the truck, yielded the maximum drag reduction of 6.551%, while multiple rectangular channels, on the sides of the truck, achieved the second highest drag

reduction (5.12%) of all add-ons. All the add-ons proposed in this study are easy and cost-effective to manufacture. Further, it can be directly used on trucks and buses without training the drivers.

ACKNOWLEDGEMENT

The authors would like to thank Kulliyah of Engineering, International Islamic University Malaysia (IIUM) for providing the computing resources.

REFERENCES

[1] FH. Hsu and RL. Davis, "Drag reduction of tractor-trailers using optimized add-on devices," *J. Fluids Eng., vol.* 132, no. 8, 084504, 2010a, doi: 10.1115/1.4001587.

[2] A. Altaf, AA. Omar, and W. Asrar, "Review of passive drag reduction techniques for bluff road vehicles," *IIUM Eng. J., vol.* 15, no. 1, pp. 61-69, 2014, doi: 10.31436/iiumej.v15i1.477.

[3] A. Altaf, AA. Omar, and W. Asrar, "Passive drag reduction of square back road vehicles," *J. Wind. Eng. Ind. Aerodyn.,* vol. 134, pp. 30–43, 2014, doi: 10.1016/j.jweia.2014.08.006.

[4] P. Gopal, and T. Senthilkumar, "Influence of wake characteristics of a representative car model by delaying boundary layer separation," *J. Appl. Sci. Eng.,* vol. 16, no. 4, pp. 363-374, 2013, doi: 10.6180/jase.2013.16.4.04.

[5] RP. Akshoy, J. Anuj, and A. Firoz, "Drag reduction of a passenger car using flow control techniques," *Int. J. Automot. Technol.,* vol. 20, pp. 397-410, 2019.

[6] B. Ram, and RB. Sharma, "Drag reduction of passenger car using add-on devices," *J. Aerodyn.,* 2014, 678518, doi: 10.1155/2014/678518.

[7] A. Ait Moussa, J. Fischer, and R. Yadavm, "Aerodynamic drag reduction for a generic truck using geometrically optimized rear cabin bumps," *J. Eng.,* 2015, 789475, doi: 10.1155/2015/789475.

[8] Y. Wang, C. Wu, G. Tan, and Y. Deng, "Reduction in the aerodynamic drag around a generic vehicle by using a non- smooth surface," *Proc IMechE Part D: J Automobile Engineering*, vol. 231, no. 1, pp. 1–15, 2017, doi: 10.1177/0954407016636970.

[9] G. Sivaraj, K.M. Parammasivam, and G. Suganyal, "Reduction of aerodynamic drag force for reducing fuel consumption in road vehicle using basebleed," *J. Appl. Fluid Mech.*, vol. 11, no. 6, pp. 1489-1495, 2018, doi: 10.29252/jafm.11.06.29115.

[10] AW. Huluka, and CH. Kim, "Effect of the air duct system of a simplified vehicle model aerodynamic performance," *Int. J. Automot. Mech. Eng.,* vol. 17, no. 2, pp. 7985-7995, 2020, doi: 10.15282/ijame.17.2.2020.17.0598.

[11] T. Huang, X. Zhuang, Z. Wan, and Z. Gu, "Experimental and numerical investigations of the vehicle aerodynamic drag with single-channel rear diffuser," *Proc. IMechE Part D: J Automobile Engineering*, vol. 234, no. 8, pp. 2216–2227, 2020, doi: 10.1177/0954407019893849.

[12] A. Hariram, T. Koch, B. Mardberg, and J. Kyncl, "A study in options to improve aerodynamic profile of heavy-duty vehicles in Europe," *Sustainability*, vol. 11, no. 19, pp. 5519, 2019, doi: 10.3390/su11195519.

[13] G. Rossitto, C. Sicot, V. Ferrand, J. Borée, and F. Harambat, "Influence of afterbody rounding on the pressure distribution over a fastback vehicle," *Exp Fluids*, vol. 57, no. 43, 2016, doi: 10.1007/s00348-016-2120-1.

[14] Fatima-zahra Hachimy, A.O. Ashraf, and Omar Elsayed., "The accuracy of the numerical solution in predicting Ahmed body components drag coefficients," *CFD Letters*, vol. 14, no. 5, pp. 24–32, 2022, doi: 10.37934/cfdl.14.5.2432.

[15] B.B.F. Armalyt, F. Dursts, J.C.F. Pereira, and B. Schönung, "Experimental and theoretical investigation of backward-facing step flow," *J. Fluid Mech.*, vol. 127, pp. 473-496, 1983, doi: 10.1017/S0022112083002839.

[16] G.V. Selby, "Applicability of the independence principle to subsonic turbulent flow over a swept rear facing step," *AIAA Journal*, vol. 2, pp. 1603- 1604, 1983, doi: 10.2514/3.8298.

[17] H. Le, P. Moin, and J. Kim, "Direct numerical simulation of turbulent flow over a backward-facing step," *J. Fluid Mech.*, vol. 330, pp. 349-374, 1997, doi: 10.1017/S0022112096003941.

[18] C.L. Gerald, and A.K. Walter, "Scaling of turbulent wall pressure fluctuations downstream of a rearward facing step," *J. Acoust. Soc. Am.*, vol. 107, no. 1, 2000, doi: 10.1121/1.428561.

[19] H. Park, WP. Jeon, H. Choi, and JY. Yoo, "Mixing enhancement behind a backward-facing step using tabs," *Phys. Fluids*, vol. 19, no. 10, 105103, 2007, doi: 10.1063/1.2781597.

[20] BD. Kim, and P. Moin, "Direct numerical study of air layer drag reduction phenomenon over a backward-facing step," *Center for Turbulence Research*, Stanford University, Annual Research Briefs, 351–363. 2010. Available from: https://web.stanford.edu/group/ctr/ResBriefs/2010/29_kim.pdf.

[21] F. Selimefendigil, and HF. Öztop, "Effect of a rotating cylinder in forced convection of ferrofluid over a backward facing step," *Int. J. Heat Mass Transf.*, vol. 71, pp. 142-148, 2014, doi: 10.1016/j.ijheatmasstransfer.2013.12.042.

[22] PP. Araujo, and ALT. Rezende, "Comparison of turbulence models in the flow over a backward-facing step," *International Journal of Engineering Research and Science*, vol. 3, no. 11, pp. 88-93, 2017.

[23] L. Dahai, "Numerical simulation of turbulent flow over a backward facing step using partially averaged Navier-Stokes method," *J. Mech. Sci. Technol.*, vol. 33, pp. 2137-2148, 2019.

[24] J. Rajasekaran, "On the flow characteristics behind a backward-facing step and the design of a new axisymmetric model," M. S. thesis, University of Toronto, Toronto, 2011.

[25] H.J. Park, W.P. Jeon, H. Choi, and J.Y. Yoo, "Mixing enhancement behind a backward- step. facing step using tabs," *Phys. Fluids*, vol. 19, no. 10, p. 105103, 2007. Available from: doi:10.1063/1.2781597.

[26] A.N.P. Kumar, V.D. Raju, and P.R. Kumar, "Aerodynamic studies on automobile structures," *IOSR J. Mech. Civ. Eng.*, vol. 12, no. 5, pp. 22-30, 2015.

[27] R. Rohit, CR. Kini, and G. Srinivas, "Recent trends in aerodynamic performance developments of automobile vehicles: A review," *J. Mech. Eng. Res. Dev.*, vol. 42, no. 4, pp. 206-214, 2019, doi: 10.26480/jmerd.04.2019.206.214.

[28] G. Alfonsi, "Reynolds-Averaged Navier-Stokes equations for turbulence modeling," *Appl. Mech. Rev.*, vol. 62, no. 4, 2009.

[29] D.C. Wilcox, "Formulation of the k-ω turbulence model revisited," *AIAA Journal,* vol. 46, no. 11, 2008, doi: 10.2514/1.36541.

[30] P. Gilliéron, and A. Kourta, "Aerodynamic drag reduction by vertical splitter plates," *Exp. Fluids*, vol. 48, no. 1, pp. 1–16, 2009, doi: 10.1007/s00348-009-0705-7.

[31] H. Park *et al.*, "Drag reduction in flow over a two-dimensional bluff body with a blunt trailing edge using a new passive device," *J. Fluid Mech.*, vol. 563, pp. 389, 2006. doi: 10.1017/S0022112006001364.
[32] G.K. Suryanarayana, H. Pauer, and G.E.A. Meier, "Bluff-body drag reduction by passive ventilation," *Exp. Fluids,* vol. 16, pp. 73-81, 1993.
[33] STAR-CCM+. User Guide version 3.0 2008. CD-adapco, Computational Dynamics Limited.